CFD for Better Understanding of Wind Tunnel Tests

N Qin
Department of Mechanical Engineering
University of Sheffield
Mappin Street
Sheffield S1 3JD
UK
n.qin@sheffield.ac.uk

Keywords: shock waves, vortices, parabolised Navier-Stokes, incipient separation, wind tunnel wall interference

Abstract:

In this paper, we discuss how CFD may be used for better understanding of wind tunnel tests. Three examples are used to illustrate the potential use of CFD to help the understanding of phenomena observed in the wind tunnel tests, to extend/derive simple aerodynamic criteria based on CFD, and to use CFD to improve the accuracy of wind tunnel measurements.

Introduction

CFD requires validation for complicated flow problems involving complex physics such as turbulence. Wind tunnels are still the most commonly used validation tools for CFD including physical modelling although some limited use of reliable DNS data base for simple geometries is recently becoming possible. One can observe the trend that a higher and higher demand on the accuracy of the wind tunnel measurement as numerical simulation and CFD expand into more and more complicated flow regimes. This paper gives a few examples to demonstrate how CFD may be used in a reversed way to help wind tunnel to meet the challenges posed by both better understanding of flow physics and CFD validations.

Mechanism of Windward Shock Wave Generation

For supersonic flows around slender pointed bodies of a circular cross section (an ogive shape), a bow shock form in an approximately conical shape around the geometry. At certain conditions for moderate incidences, a weak secondary wave was occasionally observed in the Schlieren images. This was initially attributed to the possible local geometrical roughness of the models or the wind tunnel walls. However the consistency of the position of the weak shock wave indicates the physical relevance of the phenomenon.

Figure 1 shows the Schlieren picture of a wind tunnel test carried out by Birch *et al*[1]. for a supersonic flow around an ogive cylinder at a moderate incidence. Clearly visible is the strong bow shock wave from the tip of the geometry. We can also see the boundary layer and vortical flow development on the leeward side of the geometry. Although some noises can easily be dismissed from the optical image, a weak secondary windward wave can be identified and seem to appear consistently in the experiments. Its consistency indicates its physical relevance. However a physical explanation needs to be found. The possibility of model imperfection was excluded at an early stage of the study. While the windward shock was clearly evident in the surface pressure and Schlieren photographs at the lower crossflow Mach numbers, it was not observed for the higher crossflow Mach number cases. All experiments were performed with turbulent boundary layers where transition was fixed close to the nose and therefore the boundary layer around the ogive is fully turbulent.

Figure 1: Schlieren Picture for Supersonic Flow around an Ogive Cylinder at M=1.8, α=14°, Re/D=6.6x10^5

In a study by Prince and Qin[2], an efficient supersonic solver based on the parabolised Navier-Stokes equation was used to investigate the mechanism for the formation of this weak windward wave in the experiments and its relation to the crossflow Mach number. An implicit space marching approach for supersonic flow problems makes the solution very efficient even for very fine grids. The numerical integration procedure yields cell average flow properties, assigned to the cell centres of each hexahedral cell. The flux vectors are evaluated at the cell interfaces as viscous and inviscid contributions. The inviscid fluxes are calculated using Osher's (P-Variant) approximate Riemann solver while the viscous and heat fluxes are evaluated using central difference. A no-slip boundary condition is employed at the wall for viscous calculations. The PNS solver assumes the far-field boundaries can be treated with a supersonic inflow boundary condition. Solution convergence is achieved by employing local time stepping with multigrid acceleration with implicit time stepping/implicit space marching. More detail on the continuous PNS solver development can be found in Qin and Richards[3], Birch *et al.*[4], Qin *et al.*[5] and Ludlow *et al.*[6]. The turbulent boundary layers are modelled using the Baldwin-Lomax approach with the modifications for crossflow separation of Degani and Schiff[7] and the Curvature approach of Qin and Jayatunga[8]. In the current study the Degani-Schiff circumferential cut-off was reduced from a value of 1.5 to a value which provided the best match with experiment, following the work of Prince[9]. Turbulent computations were carried out assuming transition at the nose tip such that the boundary layer over the whole surface is turbulent according to the experiments.

In the numerical simulation, a grid convergence study was performed using four different grids, the finest of which was 89×89×119. As the windward shock is a very weak feature, some coarse grids have totally missed it in the solution due to poor grid resolution. The windward shock was first resolved with a medium grid 60×85×60. Figure 2 presents the numerical solution on the fine grid, using a modified Degani-Schiff turbulence model, for the symmetry plane density gradient with surface skin friction lines together with a flowfield interpretation sketch. The skin friction lines indicate a shift of the primary separation line towards the windward side as the vortex shock leaves the body. The windward shock forms as a trace of the three dimensional vortex shock on the symmetry plane.

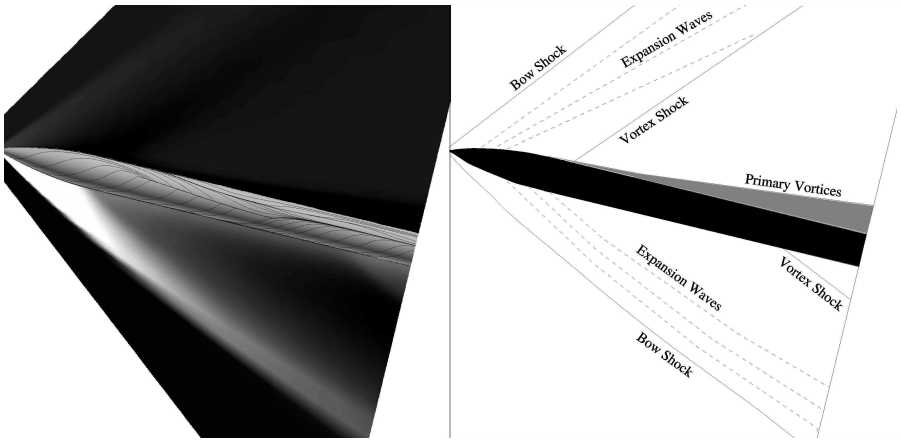

Figure 2: Computed symmetry plane density gradient ($\nabla\rho$), surface skin friction lines and interpretation.

Figure 3 presents the computed crossflow structure at a station x/D=5.5, where the embedded shock is clearly evident, together with an interpretation of the flow. The embedded shock is the manifestation of the vortex shock due to the vortical flow effects. As the flow moves downstream, the intersection of the vortex shock with the body moves further to the windward side. Eventually the vortex shock leaves the body, forming a trace on the windward symmetry plane.

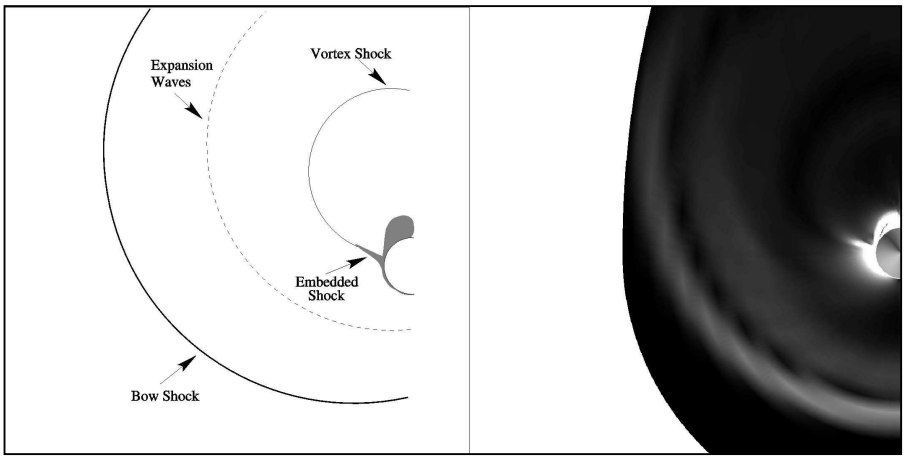

Figure 3: Computed density gradient ($\nabla\rho$) on crossflow plane at x/D=5.5, and interpretation

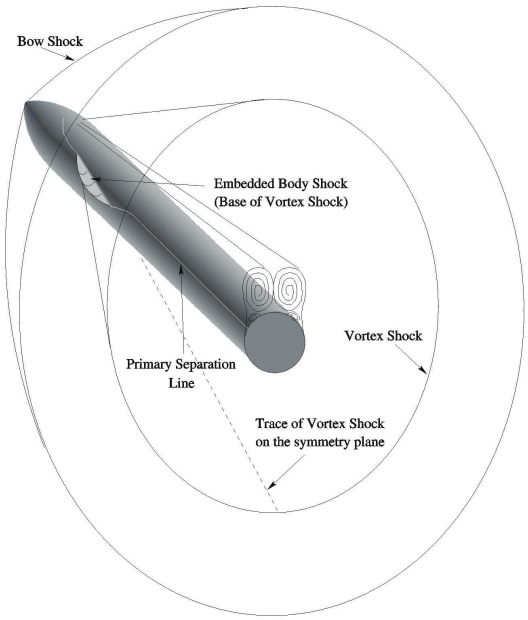

Figure 4: Shock-wave pattern for subsonic crossflow with transonic region.

A number of test cases have been conducted for various crossflow Mach numbers. To summarise, the evidence from the study of the test cases suggests that the windward shock forms because of the deflection of the supersonic flow caused by the double cone-like displacement effect of the primary vortices on the leeside body shape. The windward shock can therefore be renamed the *"vortex shock"*. In addition it would seem that the embedded shock, which appears in the crossflow, is the manifestation of the vortex shock, which is strengthened as it interacts with the body in regions of supersonic crossflow. Figure 4 illustrates the three-dimensionality of the vortex shock as interpreted in the present study.

Further studies have revealed that, under some conditions when the crossflow Mach number is relatively high, the vortex shock is sustained along the whole length of the body, inducing primary vortex separation around ϕ=90^o. This explains the disappearance of the windward shock at relatively high incidence cases. One such case is shown in Figure 5. This explains the disappearance of the windward shock at relative high incidences.

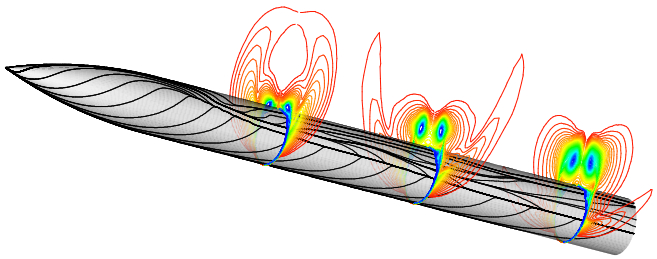

Figure 5: Computed surface skin friction pattern and pitot pressure contours at three crossflow planes for M=2.5, a=14º, Re/D=1.23x10^6

On the other hand, there are also situations when multiple windward shocks may appear due to the generation of multiple vortex shocks under certain flow conditions. Figure 6 shows such a case tested by Esch[10] along with the PNS solution, which is able to capture both vortex shocks (therefore windward shocks) and their traces on the surface skin friction lines. There is a double shift of the primary separation lines as the trace of the double vortex shocks.

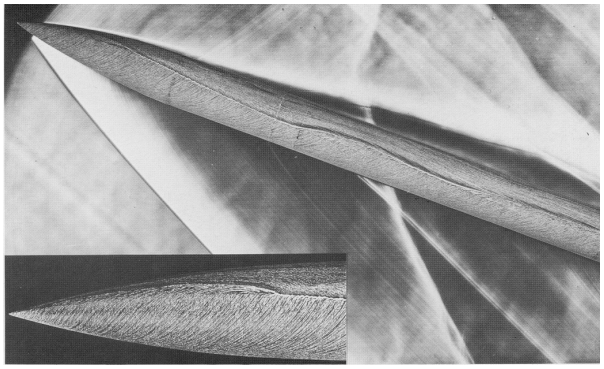

a) Experimental composite Schlieren/Oil flow photograph

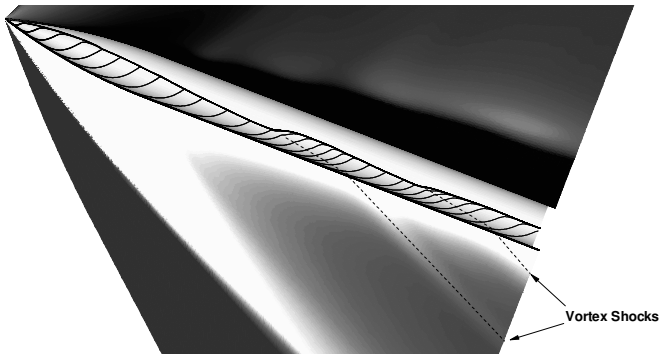

b) Predicted symmetry plane density gradient ($\nabla\rho$) and surface skin friction lines

Figure 6: Comparison of experimental oil flow results and computed surface skin friction pattern for M=1.5, α=21.2º, Re/D=1.2x10^6 .

This example highlights the usefulness of CFD numerical simulations in helping us to understand flow phenomena, especially those weak features difficult to be identified in wind tunnel tests. Careful numerical study including grid sensitivity and turbulence model effects is crucial to capture these unknown weak features, some of which can be significant in design.

Criterion for Incipient Separation

Various simple empirical aerodynamic models were developed based on wind tunnel tests and aerodynamic analyses. The criterion for incipient separation is one of these simple empirical models.

Criteria for incipient separation are important for control surface design at supersonic and hypersonic speeds. Empirical relations have been established based on extensive experimental tests for both laminar and turbulence flows. On the other hand, the incipient separation angle can be found by solving a non-linear problem for zero-skin friction as a function of the ramp angle based on the flow field simulation. With reliable numerical simulations for the laminar flows, we can demonstrate that, using a bi-section method, the incipient separation predicted is in good agreement with the empirical criterion. This example shows the usefulness of the CFD simulations in verifying and potentially extending the range of applicability of some wind tunnel based empirical relations. Furthermore, new *numerical* empirical relations may be derived for fast design and *real time* predictions based large credible CFD database.

Based on simple dimensional arguments and knowledge of the important parameters governing strong viscous interactions, Needlham and Stollery[11] and Holden[12] proposed an empirical correlation for incipient separation due to interactions of a shock wave and a laminar boundary layer (both inspired by a suggestion from J.G. Hall at Cornell Aero Labs)

$$M\beta_i = k\chi^{\frac{1}{2}} \tag{1}$$

where χ is the viscous interaction parameter, $M^3Re_L^{-1/2}$, k is the proportional constant varying between 70 ~ 80 depending to some extent on the wall temperature condition. This oft-cited criterion has withstood the test of time in successfully correlating a substantial body of experimental data.

Hankey[13] analysed the incipient separation problem using an approximate closed form solution for shock/boundary layer interactions and established an approximate magnitude of the proportionality of 74 for Eq.(1) for cold wall cases. Inger[5] has recently given a theoretical foundation of the empirical correlation, Eq.(1), using the triple deck theory in the high Re limit.

In a study carried out by the author[14], the incipient separation condition was investigated as a design parameter using a high resolution Navier-Stokes solution. As a result of the Navier-Stokes solution, the skin friction distribution along the wall can be calculated and whether the flow is attached or separated can then be determined. A non-linear formulation is proposed based on the skin friction calculated from the Navier-Stokes solution to find the incipient separation boundary. In the present note, we consider the combined effects of the incidence and the flap angle of a control surface on incipient separation in a hypersonic laminar flow.

A high resolution scheme for the laminar two dimensional compressible Navier-Stokes solution is required for an accurate account of the shock/boundary layer interaction. The flow solver is based on Osher's approximate Riemann solver, which has demonstrated an excellent capability for capturing both the shock waves and shear layers in the flowfield.

The flow problem is a hypersonic laminar flow at incidence over a two dimensional flat plate with a deflected flap, Fig.7.

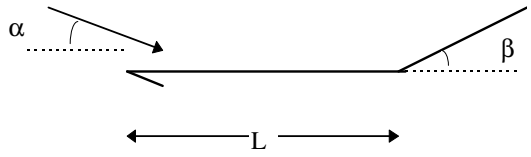

Figure 7: Sketch of the Geometry

With a fixed flap angle □, the effect of flat plate incidence □against the incoming flow on separation is studied. The incidence has an effect of decreasing the local Mach number and increasing, if the incidence is not too high, the local Reynolds number. According to the empirical formula Eq.(1), both of these changes will promote separation.

The objective of the present numerical study is to find the incipient incidence angle α_i for a given flap deflection angle β when the minimum value for skin friction along the wall is zero. In other words, given □, the following non-linear equation is to be solved for α_i

$$CFmin(\alpha) = \min_x CF(x, \alpha) = 0 \tag{2}$$

The evaluation of the non-linear function CFmin involves the solution of the Navier-Stokes equations under the given conditions. As it is difficult to get the analytical expression for the derivative of the above non-linear equation, the bisection method is used to solve the non-linear problem (2). The formulation is written as:

Find two initial approximations α_0, α_i such that CFmin(α_0)CFmin(α_i)<0.
Define $a=\alpha_0$ and $b=\alpha_i$,
for n=2, 3, ... ;
$\alpha_n=(a+b)/2$
Calculate CFmin(α_n),
if CFmin(α_n)>0, $a=\alpha_n$
if CFmin(α_n)<0, $b=\alpha_n$
until either Cfmin(α_n) or |b-a| is smaller than its given tolerance.

Due to the nature of the physical problem, we can easily find a relatively small $\alpha_0$such that Cfmin(α_0)>0 (not separated) and a relatively large $\alpha_1$such that Cfmin(α_1)<0 (separated) as the incidence promotes separation. This method does not rely on derivative information and has been found to be much more robust than the secant method for the present problem.

Results are presented in Figs.8-11 for a hypersonic laminar flow with M=12.3 and Re/cm=33000 over a control surface with the flat plate length L=15.9 cm and the flap angle $\beta=7^o$. The wall temperature T_w is 288 K and the temperature of the incoming flow T_∞ is 41.8 K. These flow conditions correspond to one set of conditions in the College of Aeronautics hypersonic gun tunnel. The incipient separation incidence α_i was found to be 3.8^o after 10 iterations. In each iteration, a steady state Navier-Stokes solution was found after the residual drops four orders of magnitude.

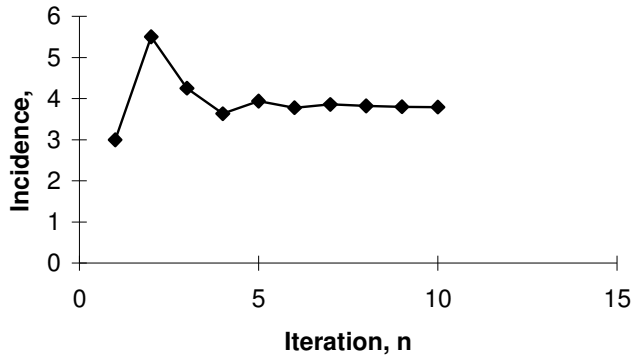

Figure 8: Convergence of Incidence to Incipient Condition

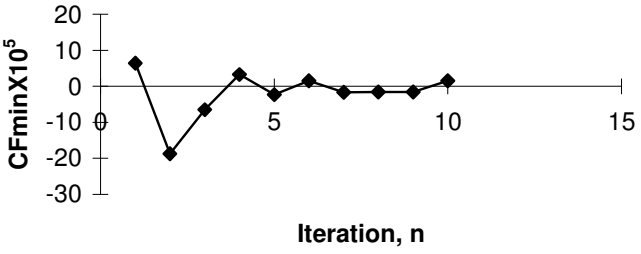

Figure 9: Convergence of CFmin

Figs.8 and 9 show the convergence of α and CFmin against the iteration number n. An acceptable result was obtained at the 6th iteration. As can be seen from Fig.9, further iterations do not produce better results(a lower CFmin) due to the rounding errors in calculating Cfmin from the Navier-Stokes solution. Figs.10 and 11 show the skin friction and heat transfer distribution at the incipient separation condition, where both curves exhibit cusp-like distributions near the hinge line.

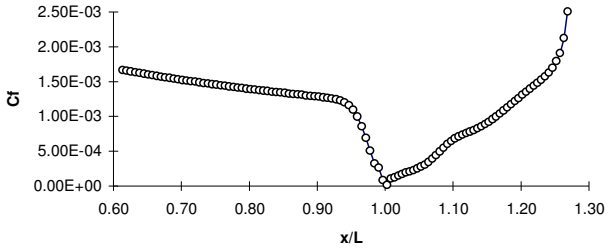

Figure 10: Skin Friction Coefficient Distribution at Incipient Condition

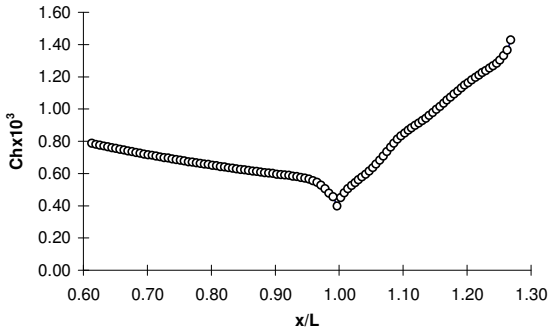

Figure 11: Heat Transfer Coefficient Distribution at Incipient Condition

Changing the flap angle β results in a corresponding change in the incipient incidence angle α using the above solution procedure. The flap deflection angles of β=6º and β=8º are also solved for the incipient incidence α_i. The resulting incipient separation boundary against the flap deflection angle and the incidence is drawn in Fig.12.

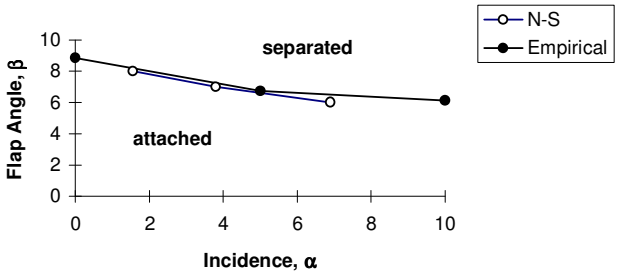

Figure 12: Incipient Separation Boundaries

Also plotted in Fig.12 is the incipient separation boundary calculated from the empirical criterion Eq.(1), where the local Mach number and Reynolds number were worked out using flow properties after the inviscid oblique shock wave corresponding to the incidence α. The constant k is taken to be 74 for the current cold wall case following Hankey. The agreement is reasonably good between the two curves though the incipient separation boundary given by the Navier-Stokes solution is slightly lower than that given by the empirical formula.

Further study along a similar line is to extend the criterion to include the wall temperature effects on incipient separation, extending the range of the application of the current empirical model. This example shows the possibility to use CFD in

generating a database for the extraction of crucial aerodynamic information in the form of simple rules, which can be very useful for the designers at the early stage of the design.

Wall Interference Assessment and Correction

Within the aerospace industry, wind tunnel tests play an important role in the design, evaluation and certification of aircraft projects. With the dramatic advance in the last few decades in computer technology and computational fluid dynamics (CFD), computer flow simulation has been increasingly used alongside with the wind tunnels to improve the product and reduce the time scale of the design cycle.

However, CFD relies on wind tunnel tests for validation of the simulated results due to two major difficulties: (1) turbulence and (2) accuracy in drag calculations. The former is due to the fact that no universal modelling exists for all the practical flow situations and direct simulation of turbulence is impractical for solving engineering problems. The latter is because of the very high sensitivity of the drag force to the grid resolution and turbulence modelling.

On the other hand, to simulate the conditions of an aircraft flying in the free air, the wind tunnel tests need to match such key parameters as the Mach number, the Reynolds number etc. as closely as possible so that the physical process is reasonably reproduced in the wind tunnel. Model sizing is a critical issue in wind tunnel testing and engineers strive to use larger models to maximise the possible Reynolds number in wind tunnels. One of the other major problems associated with the wind tunnel tests is the wall interference produced by the wind tunnel walls. It becomes stronger for larger models and for speed around to the sonic condition, i.e. in the high subsonic and low supersonic range. To alleviate the interference, perforated or slotted walls were therefore introduced for most transonic facilities.

The conflicting requirements in matching the flight Reynolds number and minimising the wall interference makes it crucial to assess and correct the wind tunnel wall interference. With confidence in the corrections, one can therefore achieve higher accuracy in the measured data for existing models or use larger models in existing tunnels to better match the flight Reynolds number. It is well-known that perforated walls weaken the wall interference at transonic speeds but the assessment of the interference is made more difficult due to the complicated boundary conditions caused by the local flow through individual holes and the resulting flow interaction. A number of researchers in the aerospace industry[15,16,17,18,19] recently developed various WIAC methods based on CFD simulations of the flow around the model in the free air and in the wind tunnel. The methodology for the correction is illustrated in Figure 13.

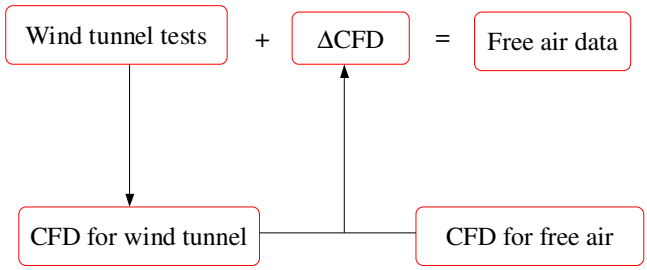

Figure 13: A diagram for CFD correction of wind tunnel data

The relative difference between the two simulations can then be used to correct the wind tunnel measurement. Key to all these methods is a proper boundary condition for the ventilated wall (perforated or slotted) in the CFD simulation, based on some empirical relations from wind tunnel data for different types of ventilated walls. McDonnell-Douglas (now Boeing) presented a perforated wall boundary condition correlating the tunnel wall surface pressure measurement with the cross flow velocity at the surface for a variety of perforated surfaces. Arnold Engineering Development Centre (AEDC) studied the cross-flow characteristics for its perforated wall wind tunnels and related the wall pressure to the local flow angle through an empirical correlation. A variety of WIAC methods can also be found in the literature for transonic tunnels with slotted walls.

In order to assess and correct the wall interference in BAE SYSTEMS' 1.2m High Speed Wind Tunnel (HSWT) with perforated walls at Warton, three Cranfield Master degree projects[20,21,22] have been carried out with sponsorship from BAE SYSTEMS. The projects studied in particular the MD method with the following achievements: (1) a CFD study of Wing 9, a 2D wing, in the free-air condition and the "ideal" porous wall condition from the free air results; (2) a wind tunnel study of Wing 9 including pressure measurement on the model surface and the wind tunnel walls; (3) a 3D wing-body study of the TWIG model in the free air and in the tunnel with the solid wall and with a full supporting structure, respectively. These

projects demonstrated the importance of the wall interference at transonic speed in the BAE HSWT. They have also show the potential of using CFD for the assessment and correction for this interference. For both the 2D Wing 9 case and the 3D TWIG case, significant wall interference has been identified at the transonic range for solid walls within the BAE HSWT. In the TWIG case, the support structure has also shown a strong effect at low supersonic speeds. These very strong wall interferences for solid walls are expected to be much weaker for the perforated walls used for the HSWT tunnel. However, as reported by MD, AEDC and NASA Langley Research Centre, significant wall interference can still occur at high subsonic and low supersonic speeds for ventilated walls even for models below 1% solid blockage ratio. Some results for the TWIG model in the HSWT wind tunnel with solid walls and a support structure are presented here.

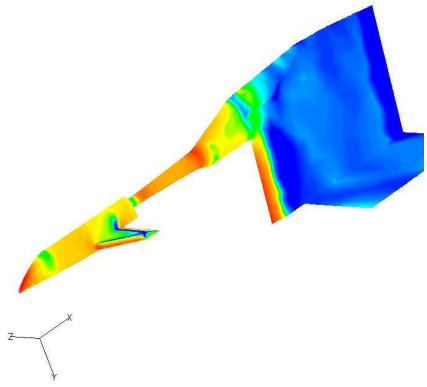

Figure 14: Pressure distribution on the TWIG model in the HSWT wind tunnel with solid wall and support, M=0.9

The above figure shows the numerically simulated pressure distribution around the TWIG model in the BAE high speed wind tunnel including the solid wall (not shown) and the support structure. It was solved with an unstructured grid using the Euler model at BAE. Only half of the geometry is solved due to symmetry. The problem was solved for a range of Mach numbers from subsonic M=0.5 to supersonic M=1.4 flow for (1) free air cases; (2) model with solid wall and (3) model with solid wall and the support structure.

Figure 15 shows the difference between the free air case (solved with far field boundary condition) and the wind tunnel solid wall case without the support structure. As can be seen, the wall interference starts at a low level at M=0.5 but becomes very high at the transonic range, reaching its peak at M=1.1. The difference drops down to near zero at higher speed at M=1.4.

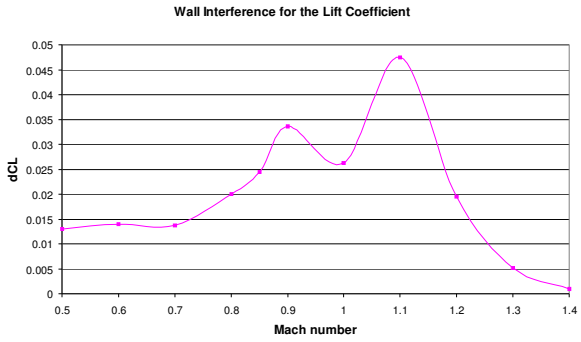

Figure 15: Lift coefficient difference between free air case and wind tunnel solid wall case

The additional interference due to the support structure is studied based on two sets of solutions for solid wall cases and solid wall with support structure. The support structure does affects the lift coefficient of the TWIG model with solid wall for Mach lower than 0.7 and greater than 1.3. The support structure shows the largest interference to the result around M=1.2.

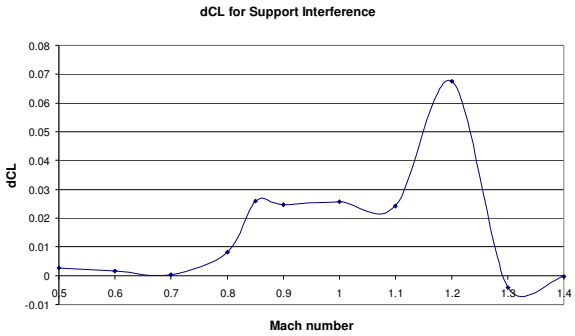

Figure 16: Lift coefficient difference between solid wall case and solid wall + support case

Figure 17 shows the comparison of the surface pressure for the three cases at M=0.9, indicating a very strong effect of the support structure at this Mach number. The solid wall effect is also visible though it is relatively small.

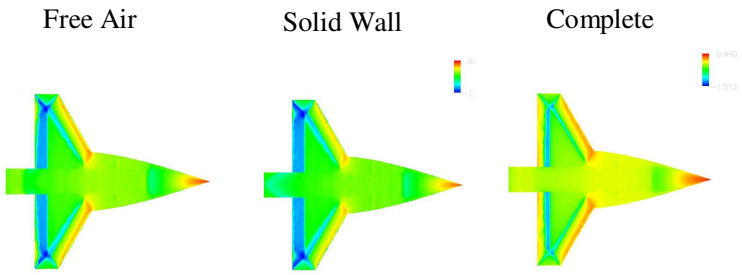

Figure 17: Upper surface pressure distribution for the three cases at M=0.9

Conclusions

The three examples shown in this paper demonstrate the capability of CFD in helping wind tunnel investigations of aerodynamic problems.

Weak flow features may be shown as anomalies in wind tunnel data or flow visualisation pictures. Detailed CFD studies with fine resolution (through fine grids or adaptive grids) can be used to identify the physical relevance (or irrelevance) of these features. High resolution and adaptive gridding in CFD are crucial in this respect in addition to correct physical modelling. Critical examination of the wind tunnel data and images is essential in order not to dismiss some weak but relevant physical features of the flow.

With the increasing confidence in CFD simulations, it is now possible to use CFD database in a similar way as we use the wind tunnel database for extracting key aerodynamic criteria. In addition to separation criteria, one may use CFD to study, for example, flutter boundaries, buffet onset, transition criteria, vortex breakdown, delta wing flow classification, critera for flow bifurcation, etc. Nevertheless, they are going to be much more difficult than the relatively simple example given here due to the much more complicated flow physics involved.

Wind tunnel data have helped CFD development tremendously during last four decades. Through continuous CFD validation of more and more challenging problems using wind tunnel data, confidence in CFD grows and so does the demand on the quality of wind tunnel tests. The example illustrates that CFD can be used in return to help wind tunnel tests in the respect of wall interference assessment and corrections, especially for the important transonic range, most relevant for current generation of civil transport aircraft.

Acknowledgements

The author would like to thank Simon Prince, Trevor Birch, Garry Shabolt, Kamal Fanibanda, Steve Puetz, Ken Burton and Tony Cross for their contribution to the work presented in this paper. Most of the work was carried out while the author was at Cranfield College of Aeronautics, partially supported by DERA/QinetiQ and BAE Systems.

This paper is dedicated to my PhD supervisor, colleague, and friend, Professor Bryan Richards on the occasion of his retirement after over 40 years of research and teaching in both experimental and computational aerodynamics.

Bibliography

[1] Birch T. J., Allen, J. M., and Wilcox, F. J. "Force, Surface Pressure and Flowfield Measurements on Slender Missile Configurations at Supersonic Speeds", AIAA Paper 2000-4207, August 2000.
[2] Prince, S.P. and Qin, N., Mechanism of windward vortex shocks about supersonic slender bodies, The Aeronautical Journal of the Royal Aeronautical Society, in print, 2002. ISSN 0001-9240.
[3] Qin, N. and Richards, B.E., Finite volume 3DNS and PNS solutions of hypersonic viscous flow around a delta wing using Osher's flux difference splitting. *Workshop on Hypersonic Flows for Re-entry Problems, Part II*, Vol.2, Springer-Verlag**,** 1991, pp947-959.
[4] Birch, T.J., Qin, N., and Jin, X., Computation of supersonic viscous flows around a slender body at incidence. *AIAA 12th Applied Aerodynamic Conference*, 1994, AIAA paper 94-1938.
[5] Qin, N. Zhong, B., Ludlow, D.K., Shaw, S.T., and Birch, T.J., Multigrid acceleration of a matrix-free preconditioned GMRES implicit PNS solver, *AIAA 37th Aerospace Science Meeting*, 1999, AIAA 99-0779.
[6] Ludlow, D.K., Qin, N. and Birch, T.J., Towards a robust, efficient and accurate numerical solver for super/hypersonic flows over arbitrary geometries, 22nd International Congress of Aeronautical Sciences, Harrogate, August 2000.
[7] Degani, D. and Schiff, L. B. "Computation of Turbulent Supersonic Flows around Pointed Bodies Having Crossflow Separation". J. Comp. Phys. 66, 173-196, 1986
[8] Qin, N. and Jayatunga, C. "Algebraic Turbulence Modelling for Vortical Flows around Slender Bodies". Paper 20, NATO, RTO MP-5, AVT Symposium on Missile Aerodynamics, Sorrento, May 1998.
[9] Prince, S. A. "The Aerodynamics of High Speed Aerial Weapons". PhD Thesis, Cranfield College of Aeronautics, September 1999.
[10] Esch H. "Wind Tunnel Investigations of the Appearance of Shocks in the Windward Region of Bodies with Circular Cross Section at Angle of Attack". DLR-Forschungsbericht 90-15, 1990.
[11] Needham, D.A. and Stollery, J.L. Hypersonic studies of incipient separation and separated Flows, AGARD CP-4, "Separated Flows", Part I, 1966, pp89-120.
[12] Holden, M.S. Theoretical and experimental studies of separated flows induced by shock-wave-boundary-layer-interaction, AGARD CP-4, "Separated Flows", Part I, 1966, pp147-180.
[13] Hankey, W.L. Prediction of incipient separation in shock-boundary-layer interactions," AIAA J, 1967, **5**, (2), pp355-356
[14] N. Qin, Incipient separation boundary: confirmation of an empirical formula by Navier-Stokes solutions. The Aeronautical Journal of the Royal Aeronautical Society, Vol.100, No.999, 1996, pp381-386.
[15] AGARD-AG-336, Wind Tunnel Wall Correction, October 1998. Chapter 5.
[16] Crites, R. and Rueger, M., Modeling the ventilated wind tunnel wall, AIAA 92-0035.
[17] Rueger, M. and Crites, R., Wind tunnel boundary interference prediction and correction, AIAA 92-0036.
[18] Jacocks, J.L., Aerodynamic characteristics of perforated walls for transonic wind tunnels, AEDC-TR-77-61, 1977.
[19] Martin, F.W. Jr., Sickles, W.L. and Stanley, S.A., Transonic wind tunnel wall interference analysis for the space shuttle launch vehicle, AIAA Paper 93-0420.
[20] Shadbolt, G., A specification and investigation of a methodology to quantify ventilated wind tunnel wall interference, MSc Thesis, College of Aeronautics, Cranfield University, February 1998.
[21] Fanibanda, K., Investigation into the application of CFD in the evaluation of boundary interference correction for a ventilated transonic wind tunnel, MSc Thesis, College of Aeronautics, Cranfield University, September 1999.
[22] Puetz, S.C., CFD studies of free air and wind tunnel flow around the DLR "Transonic Wall Interference Generator" model, September 1999.